

Mechanism for laser-induced fluorescence signal generation in a nanoparticle-seeded flow for planar flame thermometry

D. H. Gu · Z. W. Sun · P. R. Medwell · Z. T. Alwahabi ·
B. B. Dally · G. J. Nathan

Received: 14 June 2014 / Accepted: 6 December 2014 / Published online: 17 December 2014
© Springer-Verlag Berlin Heidelberg 2014

Abstract The mechanism of atomic indium generation for laser-induced fluorescence (LIF) of indium from laser ablation seeding was investigated in a hydrogen/nitrogen non-premixed flame. The morphology and particle size distributions of the ablation products were examined with scanning electron microscopy and transmission electron microscopy. These investigations show that the ablation products comprise complex agglomerates of nano-sized primary particles of indium compounds and micron-sized spherical indium beads. Images of the atomic indium LIF, Mie scattering of ablation products and natural fluorescence emission of indium in the flame were recorded to investigate the mechanism of fluorescence signal generation. The relative contribution of natural fluorescence emission of indium towards the total indium fluorescence signal was assessed by comparing these images. These images also reveal the evolution of ablation products through the flame structure and the correlation between LIF signal and ablation products. It is found that the LIF signal generation is associated with the vapourisation of indium nanoparticles into the gas phase by thermal decomposition in the flame. A further mechanism for thermal decomposition of the nanoparticles was also identified, that of heating

the ablation products by in situ laser ablation. This was assessed by means of a second laser, introduced prior to the excitation laser, to reveal that the LIF signal can be enhanced by in situ laser ablation, particularly in the upstream regions of the flame. These findings supersede the mechanism deduced previously by the authors that neutral atomic indium can survive a convection time of the order of tens of seconds and be directly seeded into reacting or non-reacting flows. The possible influences of laser ablation seeding on the nonlinear two-line atomic fluorescence thermometry technique were also assessed.

1 Introduction

Planar two-line atomic fluorescence (TLAF) of indium, seeded into a flame, is an emerging technique for providing non-intrusive and two-dimensional temperature measurements in turbulent reacting flows. It is particularly relevant in conditions where interference from Mie scattering from soot or other particles hinders the application of most optical methods [1, 2]. Sub-millimetre spatial resolution and an imaging time in tens of nano-seconds make it well suited to thermometry in turbulent flames. Indium has been identified as the preferred seeding species owing to its good sensitivity over the temperature range 800–2,800 K [3]. Engström et al. [3] and Nygren et al. [4] have previously performed several studies on simple burner configurations and Kaminski et al. [5] reported measurements in an internal combustion engine. More recently, Medwell et al. [6] extended TLAF to the nonlinear excitation regime, so called nonlinear two-line atomic fluorescence (NTLAF), to achieve sufficient signal-to-noise ratio (SNR) for single-shot imaging [7, 8] and demonstrated TLAF's relevance to application in turbulent sooty flames. High-repetition

D. H. Gu (✉) · Z. W. Sun · P. R. Medwell · Z. T. Alwahabi ·
B. B. Dally · G. J. Nathan
Centre for Energy Technology, The University of Adelaide,
Adelaide, SA 5005, Australia
e-mail: dahe.gu@adelaide.edu.au

D. H. Gu · Z. W. Sun · P. R. Medwell · B. B. Dally · G. J. Nathan
School of Mechanical Engineering, The University of Adelaide,
Adelaide, SA 5005, Australia

Z. T. Alwahabi
School of Chemical Engineering, The University of Adelaide,
Adelaide, SA 5005, Australia

rate (3.5 kHz) thermometry by TLAF in laminar methane/air flames using diode lasers has been performed by Christie et al. [9]. The feasibility of using diode laser to perform TLAF temperature measurements in low-pressure sooty flames has been demonstrated by Burns et al. [10]. However, a key challenge identified throughout these various experiments is the challenge of seeding indium atoms into the flames, while minimizing influences on the flame. For this reason, the objective of the present investigation is to address this challenge through new understanding of the mechanisms of seeding associated with an innovative approach to seeding based on laser ablation [6, 11, 12].

The desirable characteristics for a TLAF seeding technique are: (1) it achieves a uniform distribution of atomic indium throughout the flame, (2) it imposes a negligible disturbance on the flame temperature and chemistry, and (3) it achieves a high SNR and that it offers a low measurement uncertainty. To achieve these seeding characteristics with atomic indium is a particular challenge. This is well illustrated by the limitations of the dominant seeding method, in which an ultrasonic nebuliser is used to generate fine droplets of indium chloride (InCl_3), dissolved in a solvent with a typical concentration varying between 100 and 6,000 mg/L [3–5, 9, 10]. The droplets are then filtered by a droplet selector [5] to avoid seeding large droplets into the flame and transported by a carrier gas stream into the flame. The concentration of indium salt dissolved in the solution and the amount of solvent being seeded into the flame is selected to generate enough laser-induced fluorescence (LIF) signal in the flame for a good SNR, while keeping the quantity of seeded indium and solvent to a minimum. The disadvantage of this seeding approach is that the solvent inevitably changes the flame temperature, the stoichiometry and/or the soot concentration over that of the parent fuel. The flame temperature is changed because thermal energy is required to evaporate the droplets to produce atomic indium, which can also generate local thermal gradients, while the addition of solvents such as methanol or distilled water, typically reduces sooting propensity [13, 14]. For example, Engström et al. [3] reported a flame temperature reduction of 100–150 K in an acetylene/air flame, due to the addition of the InCl_3 aqueous solution into the flame. It should be noted that for measurements in liquid-fuelled systems, the bias can be mitigated by dissolving the indium salt in the fuel [5, 15]. In addition, the detection region is limited to the high temperature fuel rich zone, because indium is highly reactive under oxidising conditions. The temperature detection threshold is $\sim 1,000$ K [10], due to the high thermal energy required to decompose the metal salt. These limitations have driven efforts to develop alternative techniques, the major approaches of which are that of ablation seeding of nanoparticles [6, 11, 12] and that of seeding tri-methyl-indium [16]. Among them, the direct seeding of

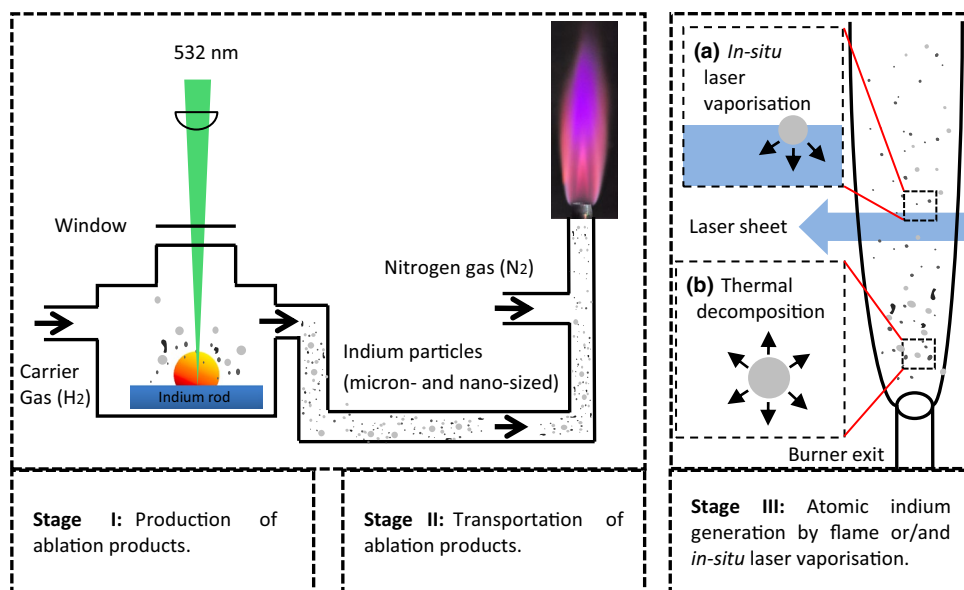
indium nanoparticles also offers the potential to seed pure indium, avoiding disadvantages of other approaches, which introduce it as a compound. The present paper is therefore directed towards advancing understanding of the ablation seeding technique, to facilitate improved thermometry in sooty flames.

Nanoparticles possess many desirable characteristics over macro-particles for direct seeding, including: lowered melting point [17], increased absorption cross-section [18], increased reactivity as a result of high specific surface area [19, 20] and high purity. Nanoparticles can be synthesised in a number of ways [21]. Laser ablation appears an attractive option because it can deliver freshly produced nanoparticles of indium into the flame by passing the fuel stream through an ablation chamber. Laser ablation involves a series of complex physical and chemical processes including thermal vapourisation, plasma ignition, expansion and cooling, particle ejection, condensation, coagulation and aggregation [22–24]. Nanoparticles are formed through the interaction between the plasma and the ambient gas, together with micron-sized particles formed from other mechanisms including solid exfoliation, hydrodynamic sputtering and liquid droplet ejection [25]. However, none of these previous investigations of laser ablation have been performed under conditions of relevance to seeding flames for NTLAF measurements. They have not been performed in a fuel atmosphere or under the combined influence of turbulent shear and convective cooling. For these reasons, there is a need for new knowledge of ablation seeding for NTLAF thermometry.

Recently, the use of laser ablation to generate ablation products from an indium rod has been demonstrated to provide a useful seeding technique for NTLAF [6, 11, 12]. The technique was shown to generate indium LIF signal at all measurement heights in the flame, including detection within the low-temperature regions of the jet flow or flame, which is not possible with nebulisation seeding. As no solvent is required, the influence of seeding on flame temperature and chemistry is significantly mitigated. Strong Mie scattering from the ablation products confirmed the presence of fine particles in the ablation products, which suggests that they may play an important role in the thermometry measurement. However, the form of the ablation products, the evolution of the ablation products through the flame and the mechanism by which neutral indium atoms, which are the target species for NTLAF, are generated in and transported through the flame, is unknown. Therefore, the uncertainty associated with ablation-seeded NTLAF is also unknown. Hence, the present paper aims to provide this understanding. More specifically, it aims:

1. To determine the size, structure and composition of the particles generated by laser ablation of indium within a gaseous fuel atmosphere;

Fig. 1 *Stage I* and *Stage II*: schematic of laser ablation seeding system. *Stage III*: two identified mechanisms responsible for atomic indium generation the flame: *a* thermal decomposition of indium nanoparticles by the hot combustion gases; *b* in situ laser vapourisation of indium nanoparticles



- To identify whether indium fluorescence is generated directly from the ablation products or whether it is derived indirectly from the conversion of the particulate matter into the gas phase;
- To identify the mechanisms by which particles are converted into the gas phase;
- To identify possible influences of laser ablation seeding on the NTLAF technique.

2 Experimental set-up

2.1 Laser ablation

The ablation products were produced using a device designed and built in-house [6]. A 10 Hz (8 ns pulse duration) 532 nm beam from an Nd:YAG laser (Continuum, Surelite II) was focused onto an indium rod. The rod was rotated and translated in a sealed ablation chamber to always provide a fresh and cooled surface for ablation products production, as shown in Fig. 1: stage I. The ablation laser energy was 0.1 J/pulse, resulting in an ablation laser fluence of 1.37×10^8 J/m². This laser energy was chosen to yield enough indium seed to give sufficient LIF signal under the current flame conditions. In addition, the dependence of the rate of generation of ablation products on ablation laser energy was measured to be linear for laser energies between 0.02 and 0.22 J/pulse. The ablation chamber was kept at approximately atmospheric pressure. Hydrogen (H₂) was used as carrier gas to transport the ablation products to the measurement volume.

2.2 Analysis of indium particles via laser ablation

Ablation products were collected to examine their morphology, elemental composition and particle size distribution. The flow rate of H₂ was 4 (standard litre) L_S/min. Ablation products were transported through a 1 m pipe onto a filter and cumulatively collected for ~30 s collection time onto a fibre filter paper or for ~2 min onto a stainless steel filter (Swagelok, 0.5- μ m pore size, thickness of 3 mm). The collection volume was kept at approximately atmospheric pressure and 300 K. Scanning electron microscopy (SEM) (FEI Quanta 450 FEG ESEM) integrated with an energy-dispersive X-ray spectrometer (EDS) was employed to perform morphology, particle size distribution and elemental composition analyses for the particulate laser ablation products. The detailed structure of particulate laser ablation products was studied using transmission electron microscopy (TEM) (Philips CM200 FEG TEM).

2.3 Burner arrangement and transportation of ablation products

Measurements were performed in a hydrogen/nitrogen jet non-premixed and unconfined jet flame at atmospheric pressure issuing from a stainless steel pipe ($ID = 4.4$ mm) into an ambient environment. This choice of fuel and conditions provides an attached soot-free flame. The use of a soot-free flame allows the location of the ablated nanoparticles to be unambiguously determined from Mie scattering, which would not be possible in a sooting flame. The use of an attached flame allows the position of the reaction zone to be known, especially near to the burner exit. The flow rate

of H_2 was 14 L_g/min, while that of nitrogen was 12 L_g/min, with an bulk exit velocity (U_e) of 28.50 m/s, which results in a Reynolds number $Re = \rho U_e d_c / \mu = 4,600$, where ρ is the density, d_c is the pipe diameter and μ is the dynamic viscosity of the fluid. This achieves a weakly turbulent flame with a visible flame length (L_f) of ~250 mm, which is well suited to easy optical access. The ablation products produced, as shown in Fig. 1: stage I were transported by the H_2 stream and mixed with the nitrogen stream before entering the flame, as shown in Fig. 1: stage II. The H_2 stream was blended with nitrogen 1 m downstream from the ablation chamber, which was 1 m upstream from the burner. A sheet of stainless steel mesh with a pore size of 0.29 mm was installed in the pipe at 0.5 m downstream from the ablation chamber to collect any large ablation products.

2.4 Optical arrangement and imaging

Imaging was performed of indium LIF, Mie scattering of ablation products and natural fluorescence emission of indium. The relative contribution of natural fluorescence towards the total fluorescence signal, the evolution of ablation products through the flame and the correlation between LIF and ablation products were assessed by comparing these images.

The optical arrangement in this study is similar to that described in earlier studies [6]. The Stokes transition of indium, at 410.18 nm, was excited using an Nd:YAG-pumped tunable dye laser (Quantel, TDL90). Indium LIF was recorded through a band-pass filter centred at 450 nm (Andover, FWHM = 10 nm). The excitation laser pulse energy was 1 mJ with sheet height of ~14 and ~0.4 mm in thickness. The Mie scattering images of ablation products were recorded through a band-pass filter centred at 410 nm (Andover, FWHM = 10 nm) by detuning the laser to 409 nm to avoid the excitation of indium fluorescence, with the same pulse energy and laser sheet dimensions as in the indium LIF measurement. Laser sheet profile corrections were performed for both the LIF and Mie scattering images. Natural fluorescence emission images were recorded without excitation by the laser. Images of the natural fluorescence emission were determined by subtracting a flame emission signal without seeding from the flame emission of a seeded flame. Both images were recorded through a band-pass filter centred at 450 nm (Andover, FWHM = 10 nm), respectively, with the same camera settings for each measurement.

To investigate the feasibility of further enhancing the LIF signal and possible influences of seeding the nanoparticles into the flames on the NTLAF technique, the effects of the use of a second, spatially overlapping laser pulse, aiming to simulate the first laser pulse in NTLAF measurement, introduced prior to the excitation laser to “preheat” the measurement volume were assessed. Both the energy of

the preheating laser and the time delay were varied independently in two studies. In both studies, the energy of the fluorescence excitation laser (410.18 nm) was kept constant at 1 mJ/pulse, while a 532 nm laser (Quantel, Brilliant B) was used to preheat the measurement volume. In the preheating laser energy study, the pulse energy of the preheating laser was varied between 2.2 and 12 mJ by inserting different ND filters in the optical path before the telescope to maintain the temporal and spatial profile of the laser beam. The time delay between the preheating laser and the excitation laser was kept at 100 ns. In the time-delay study, the time delay between two laser pulses was varied between 10 and 100,000 ns. The energy of the preheating laser was kept at 8 mJ/pulse. The fluorescence images were recorded through a band-pass filter centred at 450 nm (FWHM = 10 nm).

Images in this work were all recorded using a four intensified CCD (ICCD) camera bundle system (PCO, HFSC Pro) running in triggered single mode with a Nikon collection lens ($f_{\#} = 1.4$). The in-plane spatial resolution is 12.0 pixels per mm.

3 Results and discussion

3.1 Seeding concentration and morphology of laser ablation products

A stainless steel filter assembly was used to measure the mass flow rate of the ablation products in the carrier gas stream. Ablation products were transported with the carrier gas through a 1 m pipe, and the particulate matter was cumulatively collected for 15 min onto a metallic filter (Swagelok, 0.5- μ m pore size, thickness of 3 mm). The collection volume was kept at ambient conditions. The metallic filter assembly was weighed before and after each test using an electronic balance with measurement resolution of 0.1 mg (Mettler AE 166) to yield the average mass flow rate of all particulate matter collected by the filter. On this basis, the average concentration of particulate ablation products in the carrier gas stream delivered to the flame was estimated to be 130 μ g/g, which corresponds to a mass flow rate of indium particles into the flame of 160 μ g/min and a gas-phase mole fraction in the fuel stream of one part per million (assuming all indium particles convert to the gas phase). The thermal energy required to vapourise all the ablation products seeded into flame is negligible compared with the heat release from the flame. A conservative estimate is that the power required to vapourise the entire mass flow rate of indium particles in the flame is 6×10^{-5} % of the heat release rate (HRR) of the flame.

Figure 2a–c presents three typical SEM and TEM images of ablation products. These show that ablation products

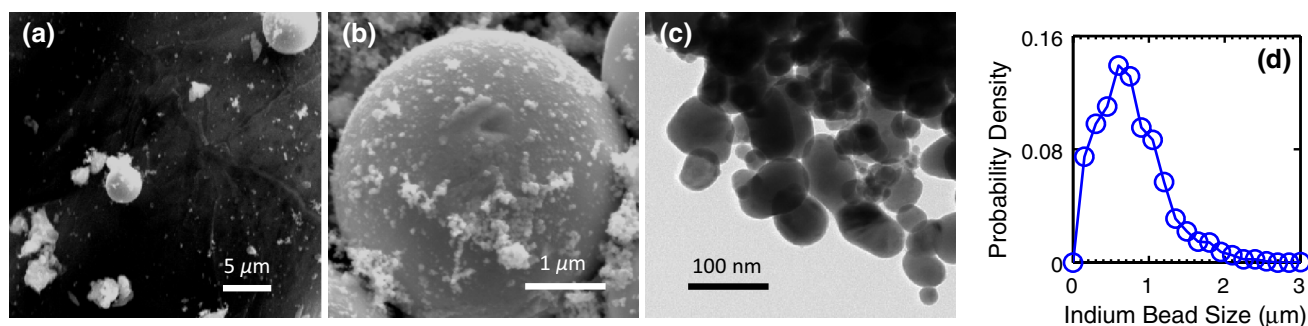


Fig. 2 Typical SEM images **a**, **b** of complex agglomerate of micron-sized spherical indium beads and nano-sized primary particles and TEM image **c** of primary particles from laser ablation of indium

are found in the form of complex agglomerates of nano-sized primary particles of indium compounds and spherical micron-sized indium beads, mainly with diameters ranging between 20–100 nm and 0.2–5 μm , respectively. Typically, each agglomerate consists of several spherical indium beads and hundreds of primary particles around the beads. Figure 2d presents the probability distribution of the diameter of the spherical indium beads measured from five SEM images, each containing approximately 1,000 indium beads. The distinct size and morphological feature of these two kinds of particles implies that the mechanisms responsible for their formation are different. The nano-sized primary particles can be deduced to form from the condensation of aerosol particles during plasma cooling which, in turn, are formed from the collision of vapourised molecules and atoms in the plasma, whereas the micron-sized indium beads result from hydrodynamic sputtering and spallation processes [26, 27]. The chemical composition of the spherical indium beads consists mostly of pure indium, while the primary particles consist of indium/hydrogen compounds, as revealed by EDS analysis.

3.2 LIF signal generation mechanism

Figure 3 presents images of (a) the natural (background) light emission from the unseeded attached flame at the same wavelength as the indium signal at 450 ± 5 nm), (b) the natural fluorescence emission from seeded indium at 451 nm (collected at 450 ± 5 nm), (c) the Mie scattering from ablation products at 409 nm (collected at 410 ± 5 nm) and (d) the LIF of indium from the seeded flame at 451 nm (collected at 450 ± 5 nm), visualised in grey scale. Images in Fig. 3 are averaged from 300 instantaneous shots. Note that the grey scale in each image is optimised separately, so their intensities should not be compared with one another.

Figure 3b presents an image of the natural fluorescence emission from the seeded flame, which is deduced to derive from chemiluminescence from reactions involving

using hydrogen as carrier gas; **d** probability distribution of the diameter of the spherical indium beads measured from SEM images

indium (the population of thermally excited indium is negligible). It can be seen that the signal intensity is below the detection limit for $x/d < 5$, which suggests that there is insufficient time in this region for the combined processes of thermal decomposition and reaction. Beyond this, the signal increases with axial distance to a maximum at $x/d = 38$, following which it decreases gradually towards zero. Importantly, the fluorescence can be seen to persist to the tip of the flame, demonstrating that this technique is effective in seeding the entire flame, as is evident from a comparison of the image of natural flame light emission (Fig. 3a) with that of the natural indium fluorescence (Fig. 3b). The natural fluorescence emission near the base of the flame can be seen to arise predominantly from the outer regions of the flame. This suggests that atomic indium is generated from the ablation products in the high-temperature regions of the flame, to be subsequently consumed in the oxidising regions. Given that the melting temperature of indium is 430 K, which is well below the flame temperature, and that the melting temperature is lower for nanoparticles than for bulk material [17], gas-phase indium can be deduced to arise from the partial vapourisation of the ablated nanoparticles. Indium has a high vapour pressure (1 kPa at 1,690 K) and a low heat of vapourisation value (241 kJ/mol), which allow it to readily vapourise from ablation particles in the flame. Very weak natural indium fluorescence is seen in the central and lower regions of the image. However, since this is a line-of-sight image, any signal from the central region of the flame includes sources generated from within the flame sheets at the “front” and “back” of the flame, as discussed in more detail later. Hence, while this image is qualitative, it is sufficient to show that the environment within the fuel rich region is a much lower source for the natural fluorescence signal than is the reaction zone. This can be explained by a combination of the relatively low temperature and a low concentration of gas-phase indium in the potential core region.

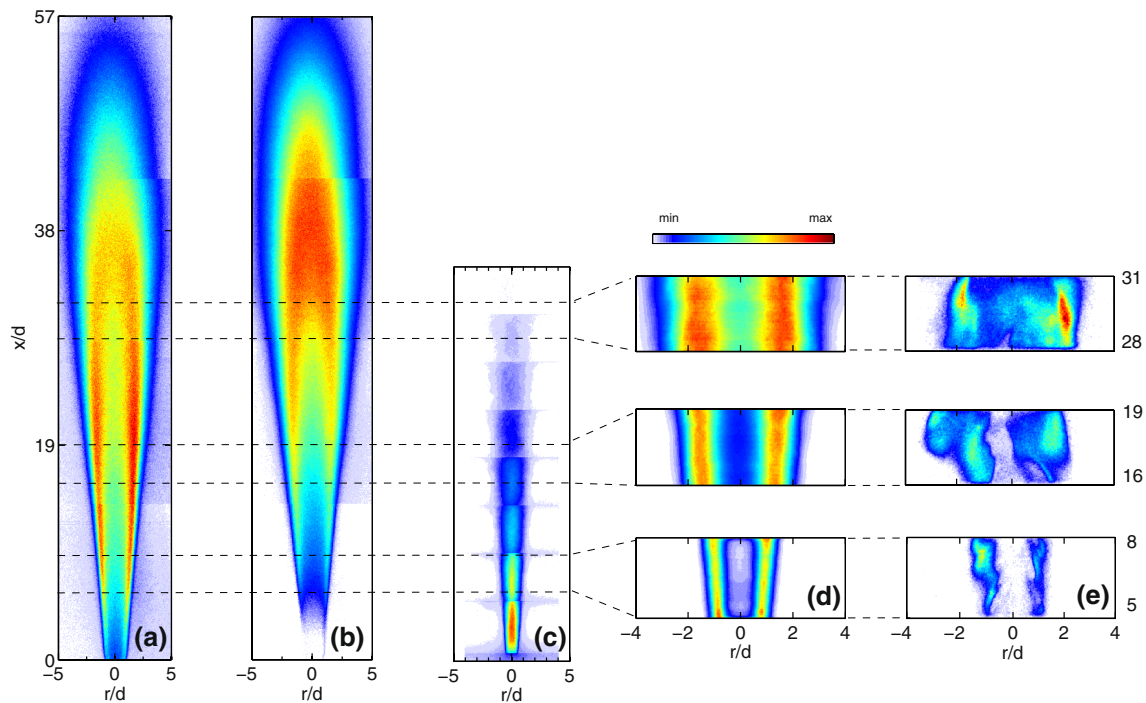


Fig. 3 **a** Averaged flame light emission image collected at 450 ± 5 nm; **b** averaged natural fluorescence image of indium from ablation products collected at 450 ± 5 nm without any laser excitation; **c** averaged laser Mie scattering image of laser ablation prod-

ucts collected at 410 ± 5 nm; **d** averaged and **e** instantaneous laser-induced fluorescence images of indium collected at 450 ± 5 nm, from the Stokes process. Hydrogen/nitrogen jet flame with an exit Reynolds number of 4,600

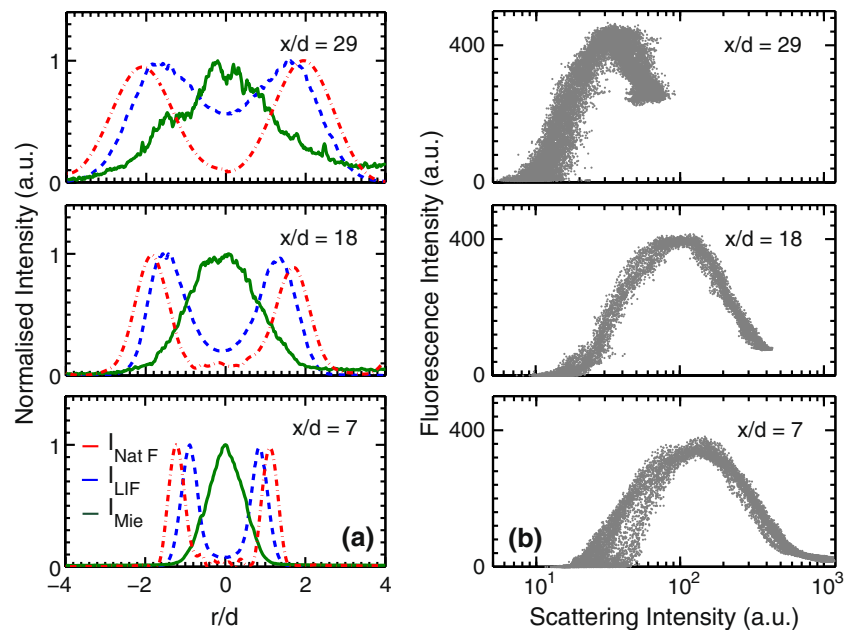
Figure 3c presents the Mie scattered signal from the ablation products in the flame. It can be seen that the particles are present immediately downstream from the nozzle exit. The Mie scattered signal is at a maximum within the jet potential core and gradually decreases in both the axial and radial directions, to be below the detection limit at an axial distance of about half of the L_f . In contrast, the natural fluorescence persists all the way to the flame tip. Together, these observations show that the particles in the downstream region evaporate to the gas phase. Similarly in the radial direction, the fluorescence can be seen to persist to a much greater extent than do the particles throughout the flame. This demonstrates that the conversion of the particulate phase to the gas phase is a key element of the laser-based seeding mechanism.

Figures 3d, e present the averaged and instantaneous indium LIF images at three different flame heights ($x/d = 7, 18$ and 29). It can be seen that the LIF signal increases with axial distance in both the averaged and instantaneous images. While there is qualitative similarity between the natural fluorescence emission and the LIF emission, as expected, especially near to the base of the flame, there are also some significant differences. These issues are addressed in more detail later.

Figure 4a compares the averaged radial profiles of natural fluorescence, Mie scattering and LIF of indium from

the seeded ablation products. The radial profile of natural fluorescence has been corrected for line-of-sight collection by performing an Abel transformation. At $x/d = 7$, it can be seen that the location of maximum concentration of ablation products, shown by the Mie scattering signal, coincides with the locations where both the natural fluorescence and the indium LIF signals are at a local minimum. Importantly, the natural fluorescence emission is close to zero on the axis, demonstrating that there is no gas-phase indium at a sufficiently high temperature to generate spontaneous emission there. In contrast, the LIF signal is low, but not zero there. This provides evidence of the laser-induced conversion of particulate matter into the gas-phase indium atoms, presumably by in situ ablation due to the LIF excitation laser. Towards the outer edge of the flame, the radial locations of the natural fluorescence peak coincide with those at which the Mie scattering has decayed to nearly zero. This suggests that the fluorescence is associated with conversion of indium nanoparticles into the gas phase by heating through the reaction zone. In addition, the LIF signals are found to occur radially inside the natural fluorescence. One possible explanation for this is the laser-induced generation of gas phase, atomic indium, from the particulate matter. However, this trend persists at $x/d = 18$ and 29 , where particulate matter has dropped to very low

Fig. 4 Radial profiles of **a** the natural fluorescence (corrected for line-of-sight imaging by performing an Abel transformation), laser Mie scattering and LIF of ablation-seeded indium; **b** joint probability distribution of LIF of indium and Mie scattering from indium particles, at $x/d = 7, 18$ and 29



levels (Fig. 3c), suggesting a different mechanism may be important. A possible explanation is that the LIF signal decreases with temperature and the source of natural fluorescence signal, chemiluminescence, increases with temperature. Therefore, the peak of natural fluorescence signal, which represents the high-temperature region, occurs outside the peak LIF signal.

Figure 4b presents the joint probability between the indium LIF signal and the Mie scattering from the ablation products calculated at each pixel over an area of 6 mm (axially) \times 35.2 mm (radially), symmetric about the centre line, at three different flame heights ($x/d = 7, 18$ and 29). It can be seen that at all heights the probability of fluorescence increases from zero with the probability of the presence of solid ablation products. This implies that fluorescence is associated with the presence of some indium particles. However, the rate of this increase declines, so that the LIF signal reaches its peak and then decreases with a further increase in the concentration of indium nanoparticles. This implies that the LIF is at a maximum where some of the nanoparticles have evaporated to the gas phase. Furthermore, the tail of this decrease becomes truncated with increased axial distance from the nozzle, consistent with the decay in maximum particle concentration with axial distance. At $x/d = 7$, the peak concentration associated with zero fluorescence shows that the presence of high concentration nanoparticles, which are only found in the potential core, is not associated with fluorescence. Some of the indium nanoparticles must be consumed to generate gas-phase indium in order for fluorescence to occur.

In addition, since indium nanoparticles have similar size and properties to soot particles, it is likely that they undergo

similar physical processes to soot particles in laser-induced incandescence (LII) measurements. A modified LII model developed by Sun et al. [28], which includes energy absorption of the excitation laser pulse and the flame, heat exchange with surrounding through conduction and radiation, has been used to evaluate the physical processes of indium nanoparticles in the flame. The effects of excitation laser fluence, combustion gas temperature and indium nanoparticle size on atomic indium release have been evaluated. Simulations support the deduction that the indium nanoparticles undergo thermal decomposition in the flame and that the excitation lasers used in NTLAF measurement can cause in situ ablation of nanoparticles to release indium atoms, as shown in Fig. 1: stage III.

3.3 Influences of laser ablation seeding on the NTLAF technique

In a NTLAF measurement [6], the typical time delay between the two excitation laser pulses is about 100 ns, to avoid strong interferences from scattered laser radiation, especially in sooty flames. The temperature measurement relies on the assumption that the number and population distribution of indium atoms in the probe volume is the same for the two successive LIF processes. This assumption is expected to be reasonable, where the indium particles have been fully thermally decomposed before the measurement, but may not be true where nanoparticles are present because the first laser pulse can generate additional atomic indium in the probe volume by in situ ablation ahead of the second pulse. To assess the effects of such in situ ablation on the NTLAF measurement, the separate influences of

excitation laser energy and time delay between the excitation lasers was investigated.

Instantaneous LIF images of the flame with and without the use of a second, spatially overlapped laser pulse, introduced 100 ns earlier than the excitation laser to “preheat” the measurement volume, are presented in Fig. 5a and b. It can be seen that the preheating laser increases the total fluorescence signal, especially in the central region at $5 < x/d < 8$ but also at $16 < x/d < 19$. The increase in signal in these regions provides evidence that gas-phase indium can be generated by in situ laser ablation of indium nanoparticles via absorption of radiation from the laser pulse, which is expected to be a broadband process. These results also show that temperature measurement in the low-temperature regions at flame positions close to the burner exit can potentially be biased by this in situ ablation process. However, because most of the region in which this bias occurs is at a temperature that is below the lower detection limit of the NTLAF technique of 800 K, the net influence of the bias is small. That is, measurements below the threshold are not included in the temperature results due to the conditional nature of the measurement. Furthermore, even in the core of the jet, the effect of in situ ablation on LIF signal diminishes with axial distance to be small at $x/d \sim 30$ and the influence is also small at the outer edges of the jet where the flame is present. This observation gives confidence that downstream flame locations, which are also of greatest interest, are unbiased by in situ laser ablation.

Figure 6a presents the results of the effects of the preheating laser energy on LIF signal at a flame position of a height above the burner (HAB) of 35.2 mm ($x/d = 8$). The data are averaged from 300 instantaneous shots, over two different areas of $0.8 \times 0.8 \text{ mm}^2$ in the flame. The two regions are located on the axis and in the reaction zone, respectively. It can be seen that both signals increase with the increase in preheating laser energy. However, the increase in LIF signal in the reaction zone is much less than the increase in the central region. This is consistent with laser-induced ablation having little influence, where the indium particles have already evaporated within the reaction zone. Noticeably, the minimum laser pulse energy employed by the preheating laser was 2.2 mJ, which is below the pulse energy of the excitation lasers normally employed in the NTLAF measurement ranging between 5 and 20 mJ. This implies in the NTLAF measurement, the excitation lasers can generate additional atomic indium in the probe volume, where the nanoparticles are present. In addition, a minimum threshold of 1.4 mJ/pulse is required before any atomic indium can be detected in the central region. This implies that in the absence of the preheating laser the concentration of indium atoms there is negligible. This implies that negligible neutral indium atoms have survived between the

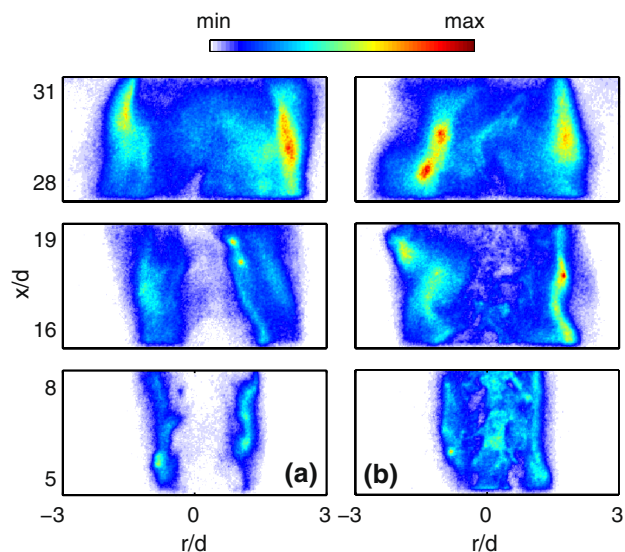
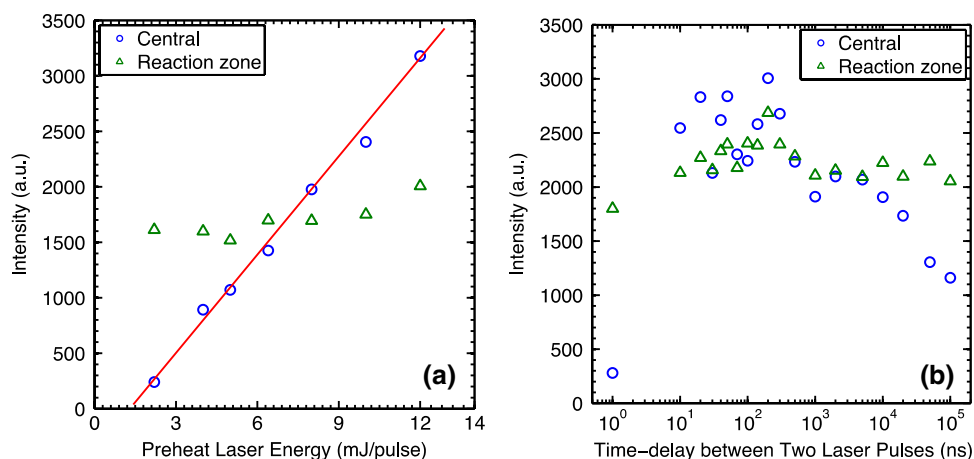


Fig. 5 Instantaneous Stokes LIF images of Indium **a** without preheating and **b** with an additional laser pulse to preheat the image volume. The colour scale in each image is the same

laser ablation seeder and the jet, which contradicts the earlier deduction by the authors [11, 12]. This does not preclude other possible mechanisms of delivering atomic indium via laser ablation-seeded products to the flame or flow.

Figure 6b presents the indium LIF signal as a function of time delay between the preheating laser and excitation laser pulses at a flame position close to the burner exit, HAB = 35.2 mm ($x/d = 8$). The data are averaged from 300 instantaneous shots, over two different areas of $0.8 \times 0.8 \text{ mm}^2$ in the flame. The two regions are located on the jet axis and in the reaction zone, respectively. The LIF signals in the reaction zone are relatively constant for a time delay of 0–300 ns, indicating the number of indium atoms in the reaction zone does not change. Therefore, the selection of time delay of 100 ns between the two laser pulses does not affect the NTLAF measurement in the reaction zone in the flame positions close to the burner exit. In contrast, the LIF signal in the relatively cold central region increases dramatically between 0 and 20 ns and starts to decrease approximately 300 ns after the start of the laser pulse, causing bias in the NTLAF measurement. The increase in LIF signal in the central regions between 0 and 20 ns is attributed to the in situ laser ablation of indium nanoparticles, while the decrease in the central region between 300 and 100,000 ns is probably due to the combination of quenching, recombination and the movement out of the interrogation region of the in situ produced indium atoms. In the reaction zone, the LIF signal level is near constant until more than 10^5 ns, indicating that equilibrium of atomic indium has been reached.

Fig. 6 Stokes fluorescence signals in either the reaction zone or the flame central region **a** as a function of preheating laser energy and **b** as a function of laser pulse temporal separation, i.e. separation of preheating and LIF excitation lasers, for HAB = 35 mm ($x/d \sim 8$)



These results also suggest that it may also be possible to avoid the bias on the temperature measurement of in situ ablation by the first pulse, by means of an additional in situ ablation laser, co-aligned with the NTLAF lasers and timed to fire slightly before the two laser pulses of the NTLAF measurement. This approach has the potential to complete the nanoparticle decomposition process in the measurement volume, with the associated release of indium atoms, before the NTLAF measurement. However, this approach would only be effective whether it can accelerate the heating rate of the particles within a region which has a temperature above the vapour temperature of indium. In addition, it would need to avoid any significant in situ heating of the measurement volume by the in situ ablation process.

4 Conclusions

The mechanism of atomic indium generation for NTLAF thermometry from laser ablation of an indium rod to generate nanoparticles has been investigated, together with the influences of this method on the NTLAF measurement.

The ablation products are found via SEM, EDS and TEM to consist of complex agglomerates of nano-sized primary particles of indium compounds and micron-sized indium beads. The nano-sized primary particles consist of indium/hydrogen compounds, while the spherical indium beads consist mostly of indium.

The ablation seeding technique is found to be effective in providing signal throughout the flame by comparison of the spatial distributions of natural fluorescence, LIF and Mie scattering in a hydrogen/nitrogen non-premixed flame. Together with joint statistical assessments, they also reveal the following new details about the seeding mechanism for NTLAF thermometry, which supersedes that deduced previously [11, 12] that neutral atomic indium can survive

a convection time of the order of tens of seconds and be directly seeded into reacting or non-reacting flows. In particular, it reveals that:

- Gas-phase atomic indium is generated within the high-temperature regions of the flame by the thermal conversion (notably by vapourisation) of nanoparticles;
- Fluorescence from raw ablation products is low without their conversion to the gas phase by thermal decomposition;
- Laser-induced in situ ablation of indium nanoparticles within the flame can be a further source of indium fluorescence. This is only significant in the low-temperature regions of the flame that are also near to the base of the flame and is expected to generally have only a small influence since such regions are mostly at a temperature that is below the threshold of the technique. Nevertheless, care must be taken in these regions to avoid any bias of the NTLAF measurement induced by a higher concentration of atomic indium in the second pulse relative to the first;
- In the low-temperature regions near the jet exit, where indium nanoparticles persist, the LIF signal in the reaction zone does not vary significantly with the time delay between the first “preheating” and excitation laser ranging between 10 and 10^5 ns. Therefore, the use of time separation of 100 ns in the NTLAF measurement will avoid any significant bias at low flame locations;
- The work also suggests that it may be possible to employ an additional preablation laser to accelerate the thermal decomposition of the ablation products within the measurement volume slightly before the NTLAF measurement at flame positions close to the burner exit. However, this would introduce a different bias on the measurement through heating the probe volume, the effect of which is not presently known.

Acknowledgments The support of the Centre for Energy Technology (CET) and The University of Adelaide is gratefully acknowledged. The support of the Australian Research Council is also gratefully acknowledged through its Discovery and LIEF schemes.

References

1. K. Kohse-Höinghaus, J.B. Jeffries, *Applied Combustion Diagnostics* (Taylor & Francis, New York, 2002)
2. G.J. Nathan, P.A.M. Kalt, Z.T. Alwahabi, B.B. Dally, P.R. Medwell, Q.N. Chan, *Prog. Energy Combust. Sci.* **38**(1), 41–61 (2012)
3. J. Engström, J. Nygren, M. Aldén, C. Kaminski, *Opt. Lett.* **25**(19), 1469–1471 (2000)
4. J. Nygren, J. Engström, J. Walewski, C. Kaminski, M. Aldén, *Meas. Sci. Technol.* **12**(8), 1294 (2001)
5. C. Kaminski, J. Engström, M. Aldén, *Proc. Combust. Inst.* **27**, 85–93 (1998)
6. P.R. Medwell, Q.N. Chan, B.B. Dally, S. Mahmoud, Z.T. Alwahabi, G.J. Nathan, *Proc. Combust. Inst.* **34**(2), 3619–3627 (2013)
7. J.W. Daily, *Prog. Energy Combust. Sci.* **23**(2), 133–199 (1997)
8. K. Kohse-Höinghaus, *Prog. Energy Combust. Sci.* **20**(3), 203–279 (1994)
9. R.S. Chrystie, I.S. Burns, J. Hult, C.F. Kaminski, *Opt. Lett.* **34**(16), 2492–2494 (2009)
10. I.S. Burns, X. Mercier, M. Wartel, R.S. Chrystie, J. Hult, C.F. Kaminski, *Proc. Combust. Inst.* **33**(1), 799–806 (2011)
11. P.R. Medwell, Q.N. Chan, B.B. Dally, Z.T. Alwahabi, S. Mahmoud, G.F. Metha, G. Nathan, *Appl. Phys. B* **107**(3), 665–668 (2012)
12. Q.N. Chan, P.R. Medwell, B.B. Dally, Z.T. Alwahabi, G.J. Nathan, *Appl. Spectrosc.* **66**(7), 803–809 (2012)
13. B. Chakraborty, R. Long, *Combust. Flame* **12**(5), 469–476 (1968)
14. I. Glassman, *Proc. Combust. Inst.* **27**, 1589–1596 (1998)
15. P.R. Medwell, A.R. Masri, P.X. Pham, B.B. Dally, G.J. Nathan, *Exp. Fluids* **55**, 1840 (2014)
16. R. Whiddon, *Application of Laser-based Diagnostics to a Prototype Gas Turbine Burner at Selected Pressures*. Ph.D. Thesis, Lund University (2014)
17. S. Lai, J. Guo, V. Petrova, G. Ramanath, L. Allen, *Phys. Rev. Lett.* **77**(1), 99 (1996)
18. R.A. Yetter, G.A. Risha, S.F. Son, *Proc. Combust. Inst.* **32**(2), 1819–1838 (2009)
19. A. Il'in, A. Gromov, V. Vereshchagin, E. Popenko, V. Surgin, H. Lehn, *Combust. Explos. Shock Waves* **37**(6), 664–668 (2001)
20. Y.-S. Kwon, A.A. Gromov, A.P. Ilyin, E.M. Popenko, G.-H. Rim, *Combust. Flame* **133**(4), 385–391 (2003)
21. F.E. Kruijs, H. Fissan, A. Peled, *J. Aerosol Sci.* **29**(5), 511–535 (1998)
22. A. Lushnikov, *J. Aerosol. Sci.* **27**, S377–S378 (1996)
23. S.B. Wen, X. Mao, R. Greif, R.E. Russo, *J. Appl. Phys.* **101**(2), 023115 (2007)
24. S.B. Wen, X. Mao, R. Greif, R.E. Russo, *J. Appl. Phys.* **101**(2), 023114 (2007)
25. C. Liu, *A Study of Particle Generation During Laser Ablation with Applications*. Ph.D. Thesis, University of California, Berkeley (2005)
26. R. Kelly, J.E. Rothenberg, *Nucl. Instrum. Methods. Phys. Res. B.* **7**, 755–763 (1985)
27. R. Webb, J. Dickinson, G. Exarhos, *Appl. Spectrosc.* **51**(5), 707–717 (1997)
28. Z.W. Sun, D.H. Gu, G.J. Nathan, Z.T. Alwahabi, B.B. Dally, in *Proceedings of the Combustion Institute*, 2014. doi:[10.1016/j.proci.2014.07.066](https://doi.org/10.1016/j.proci.2014.07.066)